Advances in Science and Technology Research Journal

Advances in Science and Technology Research Journal, 2025, 19(10), 188–198
https://doi.org/10.12913/22998624/208269
ISSN 2299-8624, License CC-BY 4.0

Received: 2025.05.20
Accepted: 2025.08.15
Published: 2025.09.01

High temperature properties of Inconel 718 parts arc-welded with tungsten electrode

Agnieszka Hotloś[1*], Grzegorz Boczkal[1], Marcin Karpiński[2]

[1] AGH University of Krakow, Faculty of Non-Ferrous Metals Al. Mickiewicza 30, 30-059 Kraków, Poland
[2] Łukasiewicz Research Network - Institute of Non-Ferrous Metals, ul. Sowińskiego 5, 44-100 Gliwice, Poland
* Corresponding author's e-mail: hotlos@agh.edu.pl

ABSTRACT

The study investigated the effect of an arc-weld made with a tungsten electrode on the mechanical properties, the specific resistivity and microstructure of Inconel 718 alloy. Static tensile tests were carried out on micro-tensile specimens deformed in a static tensile test at temperatures of 600–900 °C and as a reference at room temperature. The results showed strength properties of the joint at a level comparable to the base alloy. Mechanical stability was maintained up to 650–700 °C and deteriorated rapidly at 750 °C, where a phase transformation occurs. The microstructure in the remelting zone shows strong fragmentation of the grains and the presence of a large amount of γ"-phase (gamma double prime) precipitates forming dendritic structures. The hardness in this zone shows a decrease from 500 HV0.2 of the non-heat affected zone material to 260 HV0.2 in a fusion zone. At the same time, a decrease in the specific resistivity of the remelted material by about 10% compared to native Inconel 718 is observed.

Keywords: nickel-based superalloys, TIG welding, high temperature properties

INTRODUCTION

Nickel-based superalloys are a rapidly growing branch of materials [1, 2]. Their greatest use is in applications exposed to difficult conditions, including corrosive environments [3] and high temperature [4]. The extreme conditions inside a jet engine pose great material challenges. Nickel-based superalloys are among the best materials that can withstand these conditions for extended periods of time [5, 6]. Inconel 718 is extensively employed in the aerospace sector due to its good weldability and exceptional mechanical properties than other grades of superalloys. The high thermal strength in Inconel 718 alloy is predominantly achieved by the precipitation of γ prime – (Ni_3Ti, Ni_3Al) and γ double prime - (Ni_3Nb) phases [7]. Moreover Inconel 718 is used in the hot sections of rockets and gas turbines such as for blades, discs and casings of the high-pressure region of compressor where high temperature strength [1, 7], exceptional creep and stress rupture properties, good resistance to hot corrosion and oxidation are major requirements [7, 8]. The alloy is designed for strength, creep resistance, and good fatigue life at high temperatures of up to 700 °C [9].

The application of each material also requires appropriate joining technology [10, 11]. Joints are critical places for each alloy structure [12]. Their parameters must at least match the parameters of base material [13, 14]. The specific character of the operation of nickel-based superalloys means that any impurity can significantly reduce the parameters of the weld at high temperature [15], as elongation and strength parameters [16, 17]. To maintain the continuity of the chemical composition of the joined components, electric arc welding ignited by a tungsten electrode or special welding electrodes made of nickel-based superalloys with a composition similar to the joined materials are often used [17, 18]. The welding electrode for example, a type 112 filler electrode for Inconel alloys dedicated to joining Inconel alloys (Table 1).

Table 1. Composition of type 112 filler electrode for Inconel alloys [19]

Element	Ni+Co	C	Mn	Fe	S	Cu	Si	Cr	Nb+Ta	Mo	P	Others
Weight %	55 min	0.1 max	1.0 max	7.0 max	0.02 max	0.5 max	0.75 max	20.0-23.0	3.15-4.15	8.0-10.0	0.03 max	0.5 max

The strength of the joints made by this technique is similar to the parameters of the base material [20]. Using the fillet welding and deep penetration [21], we produced the welded structures without any harm to the strength parameters. On the other hand, changes are to be expected in both the chemical composition and microstructure of the weld zone. To eliminate impurities introduced into the weld, we decided to make the joint with a tungsten electrode. It allows for the generation of an electric arc that melts both joined elements without any change in the chemical composition of the joined material. Inconel 718 alloy exhibits good weldability compared to other grades of superalloys [23]. It can be welded either in age hardened or solution annealed condition. The weldability issues in joining of Inconel 718 alloy includes segregation of alloying elements in fusion zone (FZ) and heat affected zone (HAZ) liquation cracking and solidification cracking [22, 23].

The electrical resistivity of Inconel 718 increases linearly with temperature, starting from approximately 1.25 μΩ·m at room temperature (20 °C) and increasing to about 1.31 μΩ·m at 750 °C, showing a positive temperature coefficient [24].

The heat treatment history of Inconel 718 can significantly influence its electrical resistivity. Standard age-hardening treatments, typically performed around 720 °C followed by 620 °C, create residues that can affect electron mobility within the material [24, 25].

The reason for undertaking this research was to check the strength properties of a joint welded with a tungsten electrode at different temperatures in relation to the base material. Additionally, we examined the influence of the weld on the specific resistivity of the joint made of Inconel 718 alloy.

MATERIALS AND METHODS

The Inconel 718 alloy tested in this research is a typical representative of the nickel-based superalloys group (Table 2).

The microstructure of the Inconel 718 alloy in the state after hot rolling process was presented in Figure 1. Its microstructure includes the following phases: γ (matrix) and γ' (gamma prime) γ'' (gamma double prime) – strengthening phases [23, 27]. The grain size in the tested material was about 150 μm. The mean planar grain diameter was measured based on microstructure images using the Comparison Procedure for the base material (Inconel 718 alloy) and for the Inconel 718 alloy weld zone.

A characteristic feature was strong twinning of the microstructure inside equiaxed grains, which was a consequence of the hot rolling process.

Weld geometry and sample cutting method

Samples in the form of a 3 mm thick, 50 mm diameter Inconel 718 alloy disc were tested. The weld connecting both halves was made with a tungsten electrode by TIG welding (tungsten-inert-gas welding). Welding was performed as a both-sided operation. The welded components were put together without a gap. The welding path corresponds to the disc diameter and is approximately 10 mm wide. This is shown in Figure 2. To prepare samples, the weld surface was milled on both sides until a flat plate was obtained, cutting out next the test samples from this plate.

Chemical composition and microstructure analysis

Microstructural examinations were made with a Hitachi S3400N scanning electron microscope

Table 2. Composition and properties of Inconel 718 alloy [26]

Element	Al	C	Co	Cr	Cu	Fe	Mo	Nb	Ni	Ti
Weight %	0.52	0.021	0.11	19.06	0.02	18.15	3.04	5.08	53.0	0.93

Basic parameters	Density [g/cm^3]	Resistivity at r.t. [μΩ^{x}cm]	Rm (rolled) [MPa]	Rp02 (rolled) [MPa]	A10 [min %]
Value	8.19	127	965	550	30

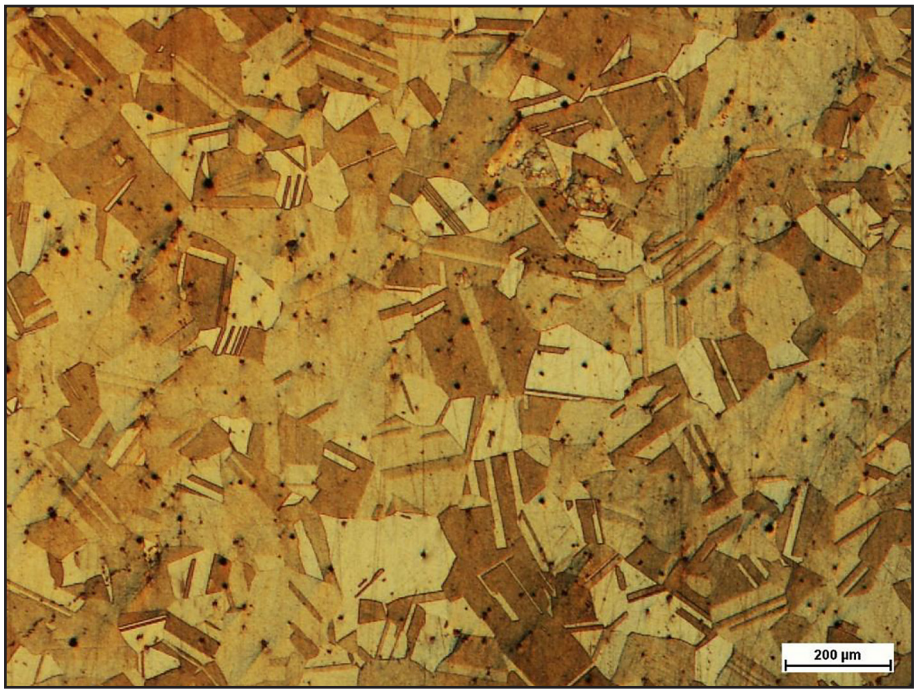

Figure 1. Microstructure of Inconel 718 alloy – base material after hot rolling process

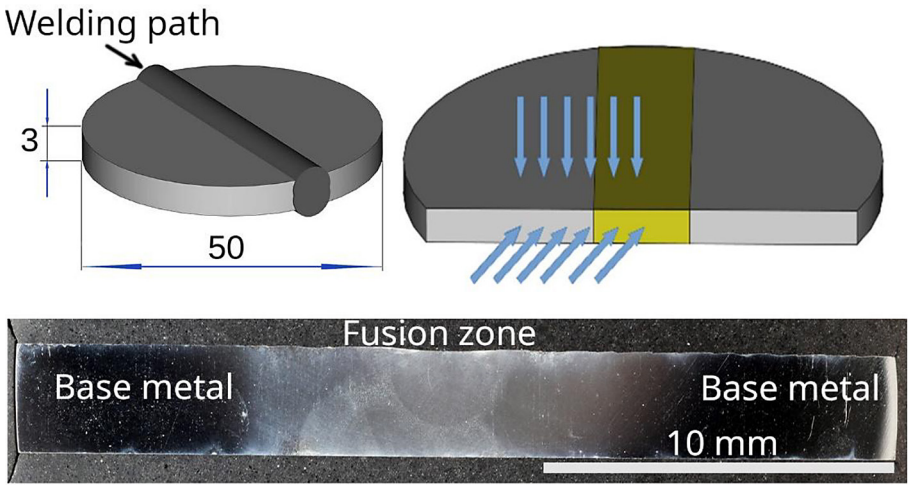

Figure 2. Schematic diagram of the weld and analysed surfaces. Bottom figure is the cross-section of the Inconel 718 weld part

with an EDS (energy-dispersive spectroscopy) chemical composition measuring attachment and a Vert.A1 Zeiss Optical Microscope equipped with the Axiocam 305 colour. Microstructures were examined at different distances from the weld (fusion zone, heat affected zone and base material). The investigations were carried out on both the disc plane and sample cross-section. This is shown in Figure 2. In selected places, on the planes longitudinal and transverse to the weld, an EDS chemical composition analysis was also performed.

Mechanical tests

Mechanical tests were performed on an Instron TM-SM model 1112 machine with a 5 kN head, equipped with grips for stretching micro-tensile specimens. The tests were carried out in a static tensile test at room temperature and at elevated temperatures ranging from 600–900 °C. The method of cutting out samples for mechanical tests is shown in Figure 3. A cuboid fragment of material was cut out from the weld zone, then the shape of the sample was cut out using the

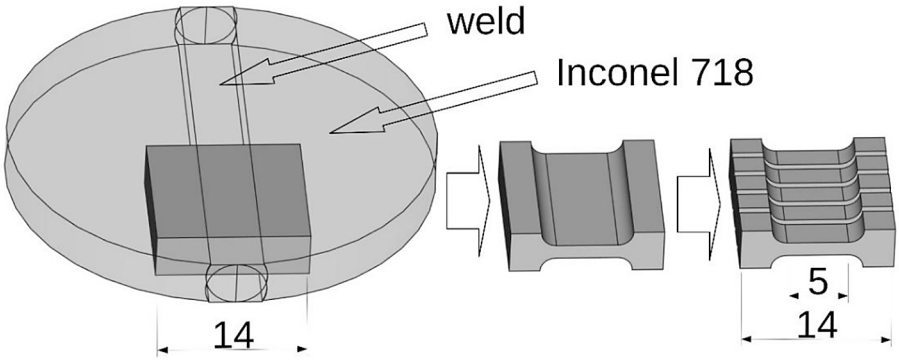

Figure 3. Preparation of the samples for high temperature tensile tests

electrical discharge machining (EDM), and in the last stage the obtained profile was cut into single samples for the tensile test.

Hardness measurements

Hardness measurements were performed with an Innovatest 240 hardness tester with a Vickers method under a load of 200 g. Measurements were taken in lines perpendicular to the welding path, with 0.25 mm spacing between indentations.

Specific resistivity measurements

Changes in specific resistivity were tested by the four-point method using a Keithley 2182A nanovoltmeter and an Agilent 34401A multimeter. An Array Electronics 3645A Programmable Linear DC Power Supply 0–36 V, 3 A was used as the power supply. Measurements were taken in the FZ (fusion zone), HAZ (heat affected zone) and base material. The current in the measuring circuit was 0.1 A. The measuring contacts were in the form of gold-plated needles equipped with a spring providing a constant pressure force of 1 N. The spacing of the measuring contacts (U1) was 2 mm. The specific resistivity measurement methodology is shown in Figure 4.

RESULTS AND DISCUSSION

The microstructure of the examined weld can be divided into several zones, as shown in Figure 5. On the left side there was the microstructure of the base material, free from the heat effect. Moving to the right, the next zone was the heat affected zone (HAZ). The another, fusion boundary zone, marks the beginning of melting caused by the electric arc. The last area on the right was the FZ (fusion zone) of the weld.

Figures 6–8 show a clearly outlined fusion boundary with changes in microstructure caused by the processes of melting and solidification taking place in the weld zone. The most visible effect was the occurrence of long dendrites (as shown in Figure 7) rich in niobium (Figure 8 shows the results of the EDS chemical composition for this area). It was a result of primary precipitation from the metallic liquid as a result of primary solidification from the weld pool. The FZ (fusion zone) exhibits a dendritic structure typical for crystallization of a nickel-based alloys during welding. The secondary dendritic arms growth is slightly inhibited due to significant cooling rate of the melt pool. High angle boundaries are typically elongated in the direction of heat source movement.

Figure 9 shows a comparative summary of the microstructure of base Inconel 718 and the microstructure of Inconel 718 after the electric arc welding process.

Base alloy was characterized by grains separated by twins boundaries and small number of precipitates. At the same time, in the fusion zone, twin structures

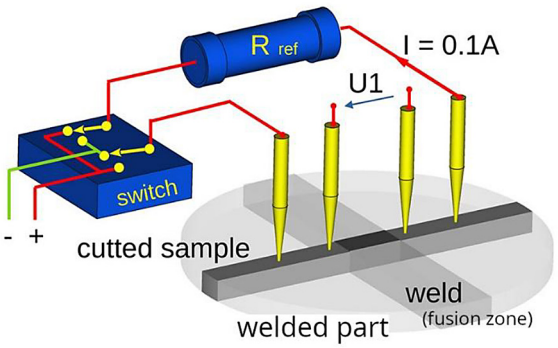

Figure 4. Samples configuration for specific resistivity measurement by 4-point method

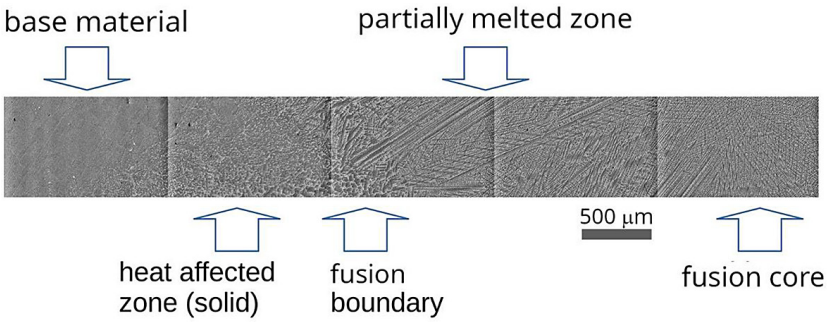

Figure 5. Microstructure evolution from base state Inconel 718 alloy to fusion zone

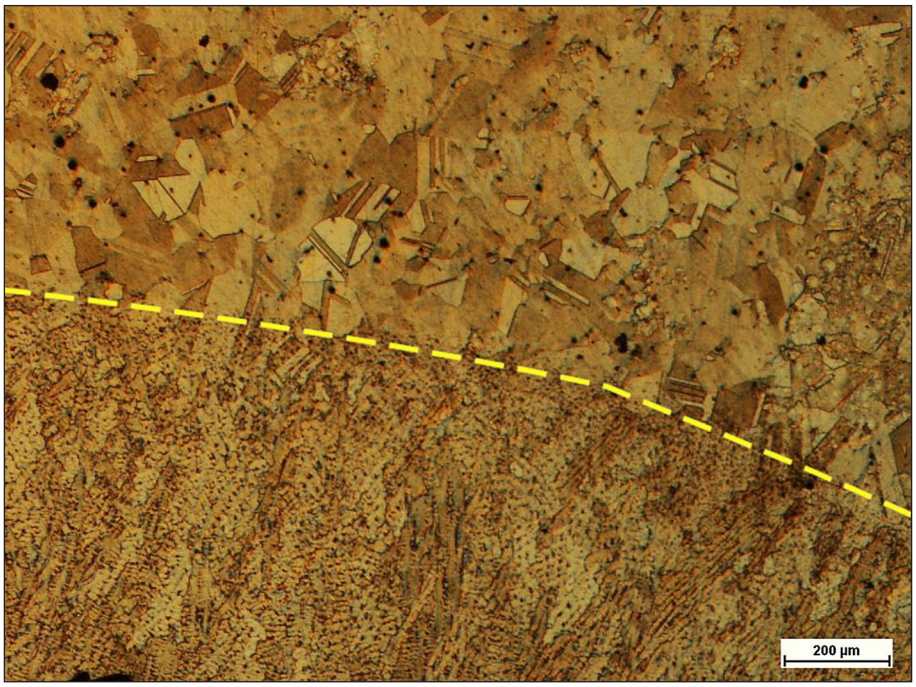

Figure 6. Boundary area between fusion zone (bottom) and base material (upper)

did not form. A large number of fine precipitates of the γ" phase was observed. At higher magnification, this area was shown in Figure 10.

A high degree of the directional ordering of microstructure was visible as a consequence of selective heat removal by both halves of the joined material.

The mean planar grain diameter has also changed. In the zone of base material it was about 150 µm with a standard deviation of about 50 micrometers, while in the weld FZ (fusion zone) the mean planar grain diameter increased to about 280 µm, but much smaller grains are observed too. The interiors of the grains are characterized by the presence of a large number of dendrites, arranged according to the orientation of the grain structure.

The EDS analysis of the chemical composition indicates that in the fusion zone there was a bright phase rich in Nb, visible at points 3,6,8 in Figure 11 and at points 3–7 in Figure 12, which indicated the presence of γ" phase.

As a result of melting of the Inconel 718 alloy in the welding process, the melted HAZ (heat affected zone) contains a strengthening γ"-phase, which was rich in Nb and transformed into the γ (matrix) and δ phases [19, 28].

Hardness measurements

The results of the hardness measurements are presented in Figure 13. The measurements were taken on a line perpendicular to the welding path direction. The results of the measurements showed an almost 50% decrease in hardness in the fusion zone, i.e. from 500 HV0.2 to about 250 HV0.2. The hardness drop area was

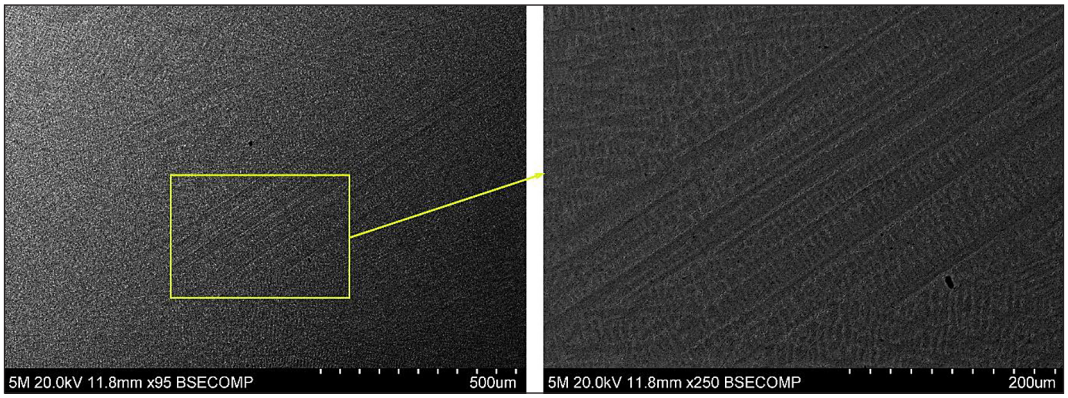

Figure 7. Macro and microstructure of long dendrites of Inconel 718 alloy in the weld zone

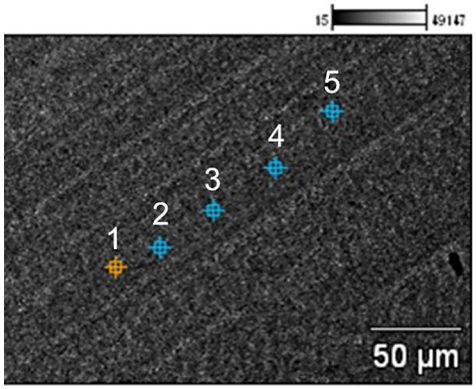

Point numer	1	2	3	4	5
Al wt %	0.68	0.40	0.79	0.60	0.82
Co wt %	0.17	0.60	0.34	0.31	0.30
Cr wt %	18.78	20.27	19.31	19.59	18.22
Fe wt %	18.88	20.51	20.14	19.99	16.26
Nb wt %	3.61	1.85	2.53	2.19	8.02
Ni wt %	54.48	53.37	54.20	52.58	51.56
Ti wt %	0.86	0.93	2.20	0.65	0.91

Figure 8. Point analysis of Inconel 718 chemical composition in the area of long dendrites

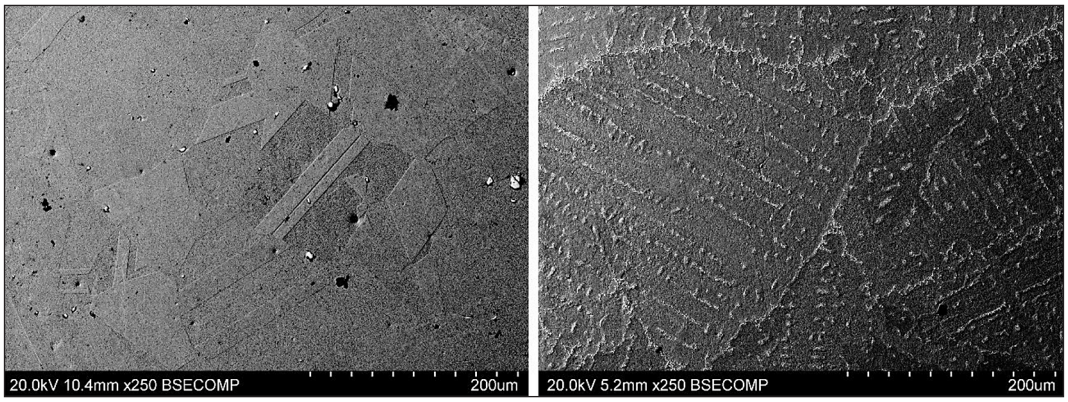

Figure 9. Microstructure of the Inconel 718, left – base material (after hot rolling processing) right – melt zone (after electric arc welding process)

approximately 12 mm wide, which corresponded to the average width of the weld observed on the macro-scale. The boundary between the two hardness areas, i.e. the base material and the melted material FZ (fusion zone), was very sharp. This was largely due to the temperature characteristics of the Inconel 718 alloy. This is an alloy dedicated to high temperature operation and its mechanical properties remain stable up to 600 °C. This causes the heat dissipation rate of the joined elements to be high enough to created a zone of strong temperature gradient between the melted phase and the solid phase. This effect was also observed in photos of the microstructure.

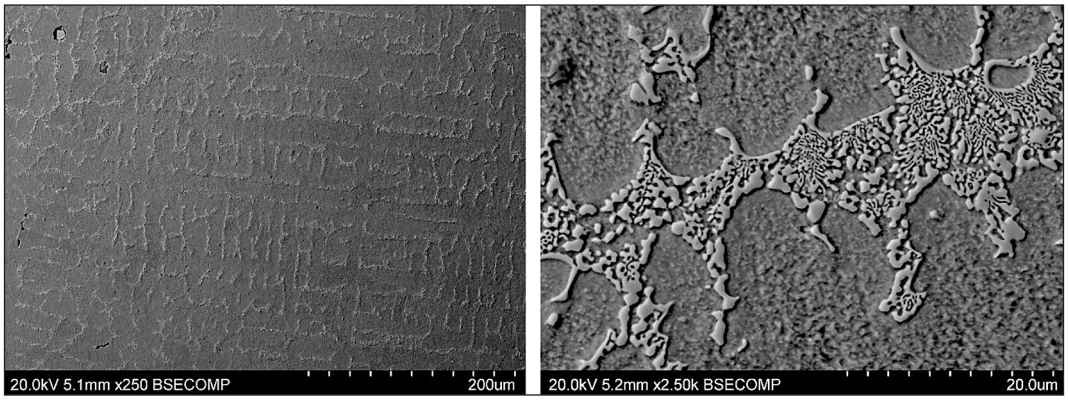

Figure 10. Long dendrites microstructure in weld zone of Inconel 718

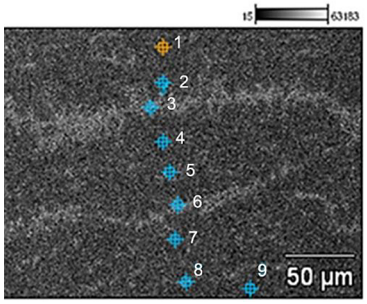

Point number	% wt							
	Al	Co	Cr	Fe	Mo	Nb	Ni	Ti
1	0.61	0.05	18.63	18.24	2.82	3.84	54.98	0.86
2	0.85	0.17	18.74	18.65	3.11	3.68	53.81	0.93
3	0.73	0.24	13.16	12.08	3.24	13.64	54.70	2.20
4	0.54	0.33	18.95	18.71	2.75	4.06	53.87	0.65
5	0.55	0.64	19.52	17.59	3.35	5.73	51.71	0.91
6	0.42	0.50	13.54	11.78	4.43	22.11	45.36	1.85
7	0.88	0.00	18.97	20.62	3.09	3.25	52.45	0.75
8	0.68	0.00	14.26	12.98	3.23	15.25	51.16	2.45
9	0.66	0.16	19.64	20.57	2.48	3.05	52.67	0.49

Figure 11. Point analysis of Inconel 718 chemical composition – weld zone

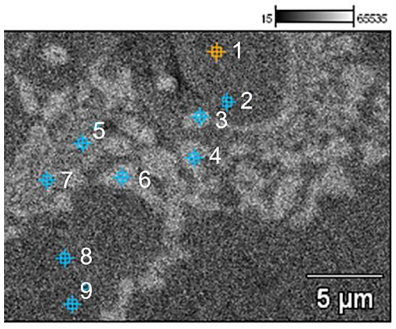

Point number	% wt							
	Al	Co	Cr	Fe	Mo	Nb	Ni	Ti
1	0.73	0.00	17.12	16.30	4.62	8.30	51.55	1.38
2	0.56	0.79	17.35	15.05	3.43	8.96	52.14	1.72
3	0.46	0.48	12.36	11.55	5.83	27.21	41.29	0.82
4	0.28	0.10	12.19	10.37	5.40	28.28	41.89	1.49
5	0.40	0.01	14.11	12.15	3.95	21.55	46.14	1.68
6	0.32	0.33	12.26	11.42	5.84	29.96	38.71	1.16
7	0.63	0.10	14.50	11.86	4.40	18.42	48.49	1.60
8	0.64	0.24	18.49	15.94	2.74	7.17	52.78	1.01
9	0.52	0.13	18.53	18.25	4.30	5.73	51.51	1.03

Figure 12. Point analysis of Inconel 718 chemical composition – fine precipitates in the weld zone

Static tensile test for different temperatures

The mechanical properties were tested at temperatures ranging from 20–900 °C. Nickel-based alloys were designed for use at elevated temperatures, and this was the reason why the focus was on testing the 600–900 °C range. The results of tensile tests at room temperature were shown in Figure 14. The results for the high-temperature tensile tests of the Inconel 718 were shown in Figure 15.

Analysis of the tensile characteristics showed that the hardening slope in the plastic region decreases with temperature. For room temperature and temperatures up to 650 °C, increasing strengthening was observed until the R_m value was reached. These curves represent typical behavior of the alloy, except at 750 °C. After exceeding this value, there was a rapid decrease in strengthening occurs and the sample broke. For these temperatures, the amount of plastic deformation reached values in the range of 10–15% elongation. We observed roughly constant tensile strength.

An increase in the test temperature above 650 °C caused a rapid change in the tensile characteristics. The R_m values remained at 600 MPa,

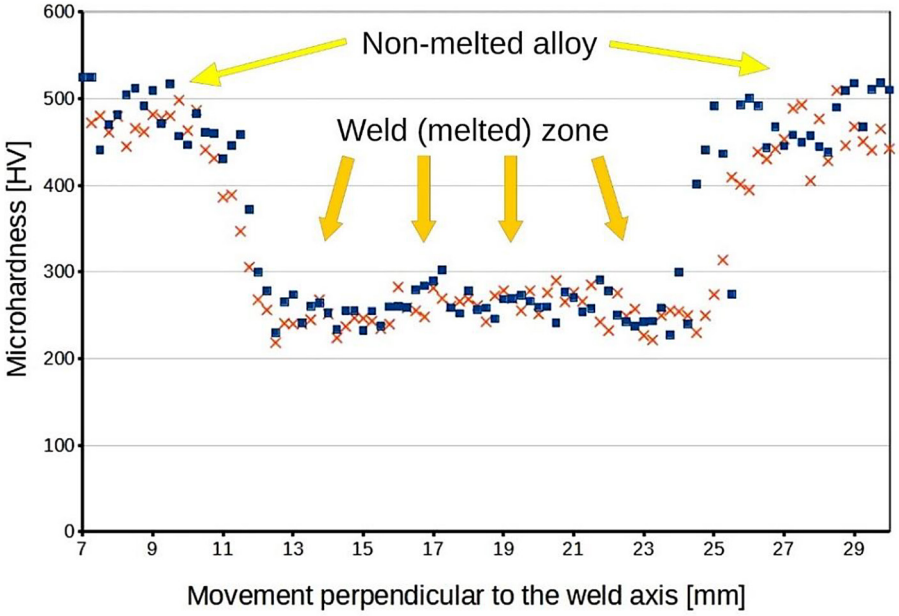

Figure 13. Hardness test perpendicular to the fusion core (weld) line

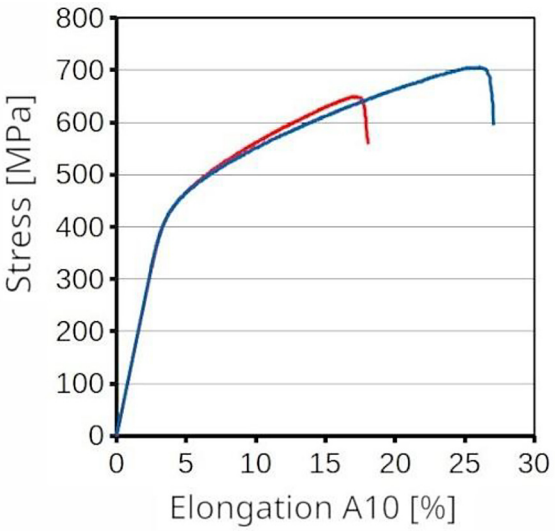

Figure 14. Results of tensile test of the welded parts at room temperature

while the plasticity range of the tested samples decreased rapidly. There was no plastic deformation range with a constant strengthening coefficient. The tensile curve was parabolic with a maximum at the R_m point. The maximum elongation didn't exceed a few percent. This situation occurred up to a temperature of 750 °C. For curves in the range of 800–900 °C, the nature of the tensile curves changed once again. The curves relation from temperature stayed typical and again showed the range of plastic deformation of the material, but this time it occurred after reaching R_m and was characterized by a negative strengthening coefficient. Elongation in this range reached about 10%, followed by a parabolic drop in stress to the breaking point.

The effects observed during the tensile test correspond to the critical points of thermal transformations in the Inconel 718 alloy. The presence of the γ'' phase was responsible for the high-performance parameters of the alloy at temperatures below 600 °C [7, 8]. This phase was durable up to the temperature of 675 °C. Over this temperature, the γ'' phase transformed into the γ' and δ phases. The effect was a rapid decrease in the plasticity of the alloy observed at temperatures of 650–700 °C. Above these temperatures, another increase in elongation was observed, but it was accompanied by a significant decrease in mechanical properties. This was due to the activation of high-temperature deformation mechanisms, such as slip at grain boundaries and high-temperature creep [29]. Owing to this, the processes of plastic deformation could occur despite the presence of hard γ (matrix) and δ phases in the alloy.

Specific resistivity test

The specific resistivity test was performed perpendicular to the welding path direction according to the diagram in Figure 16. The measuring electrode spacing of 2 mm was much smaller than the average weld width estimated at 12 mm. This allowed for a precise estimation of the changes which occur between the base material

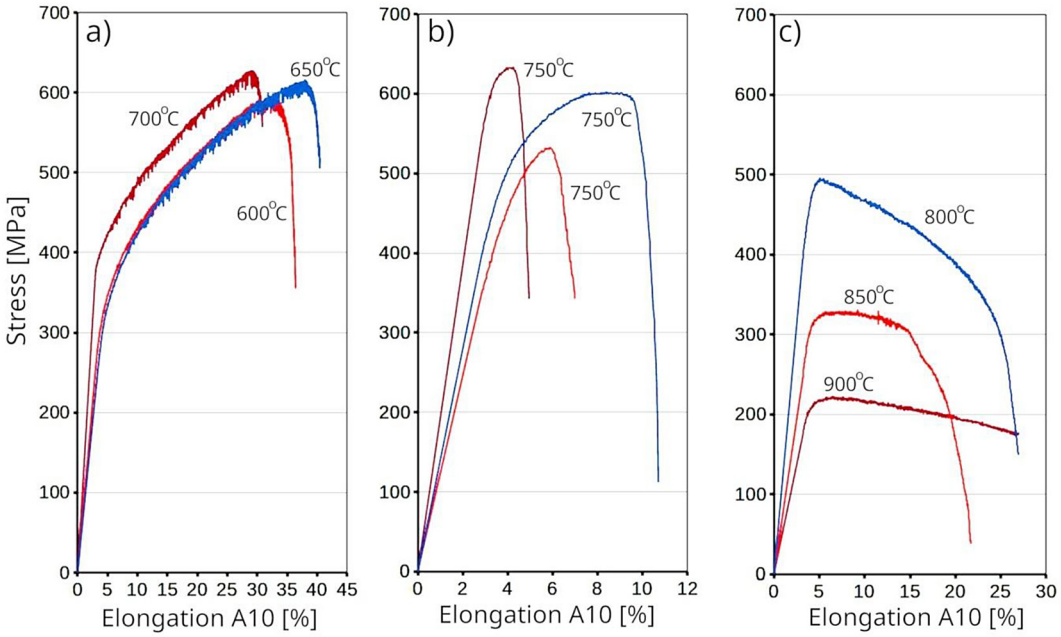

Figure 15. Inconel 718 high temperature tensile test in range of 600–900 °C.
The a) and c) figures represented averages curves, typical for specified temperatures,
b) figure illustrated instability of parameters related to the phase transition about 750 °C.

unaffected by heat and melted material in the FZ (fusion zone) on the welding path. The obtained results indicated a strong decrease in specific resistivity in the melted zone, amounting to about 15%. The causes of this phenomenon should be sought in the observed microstructural changes. The melted material included a large number of precipitates and the orientation of microstructural elements was perpendicular to the welding path direction, thus following the direction of heat dissipation by the joined halves of the material. The free path of conduction electrons in the structure had the greatest influence on specific resistivity. In the case of solid solutions, the number of dissipation centers was very large and they occur in the entire volume of the material. This shortened the free path of conduction electrons and increased the specific resistivity. With the appearance of precipitates, the structure undergoes the "cleaning" effect. The atoms of the dissolved

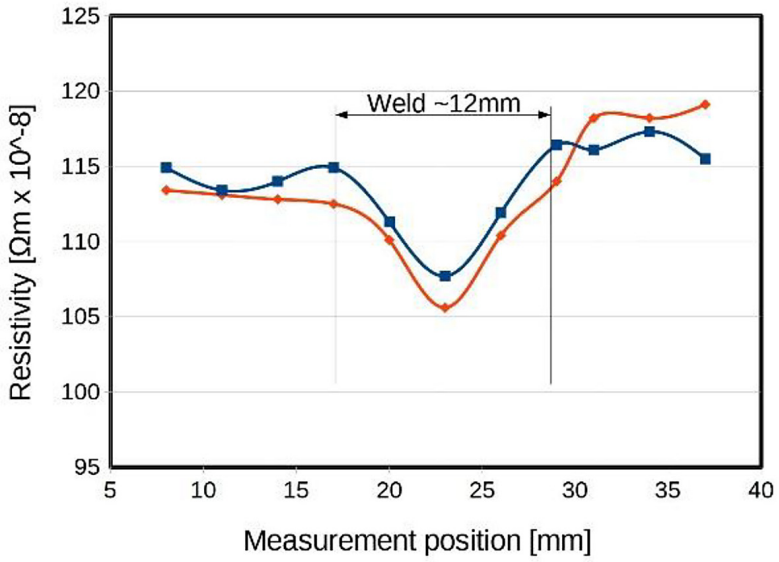

Figure 16. Specific resistivity of the Inconel 718 weld

elements concentrated in the precipitates, increasing in this way the volume fraction of the material with a longer free path of conduction electrons. Consequently, this resulted in reducing the specific resistivity. The second element favoring this phenomenon was the orientation of the microstructure following the direction of heat dissipation. This caused the formation of areas with a small number of grain boundaries and low-angle boundaries, which also leads to a decrease in specific resistivity.

CONCLUSIONS

We investigated the effect of the weld made with a tungsten electrode on the properties of the Inconel 718 alloy. Microstructural analysis showed significant changes occurring between the area of base material and FZ. The structural changes observed in the weld were typical for melted and rapidly solidifying materials. The effects of thermal gradients in the HAZ we observed. This resulted in the formation of a microstructure oriented in accordance with this phenomenon and the appearance of a large number of the γ' (gamma prime) and γ'' (gamma double prime) phases precipitates resulting from supersaturation/precipitation during the weld solidification. This was reflected in the hardness drop in the weld zone and the improvement of electrical properties.

In terms of mechanical properties at elevated temperatures, the welded material showed satisfactory mechanical properties up to a temperature of 650/700 °C. At a temperature of 750 °C, a sharp decrease in the strength and plastic properties of the material was observed due to the transformation of the γ'' (gamma double prime) phase into the γ (matrix) and δ phases. Summary, below 650 °C, γ″ strengthening dominated. Above 675 °C, $\gamma'' \rightarrow \gamma' + \delta$, causing embrittlement. This corresponded to the typical characteristics of the Inconel 718 alloy, so it can be concluded that welding with a tungsten electrode didn't significantly deteriorate the characteristics of the joined elements.

Microhardness and specific resistivity showed similar relation. In the fusion zone both of them were decreased. In case of electrical properties, reduction of the value resulted from the purification of the structure from elements dissolved in the matrix. After their transition to the precipitates, the number of conduction electron scattering centres decreased, which reduced the specific resistivity value.

The same cause caused the drop in hardness. The melting of the material during welding process resulted in the dissolution of a significant amount of the phase γ″ and also cancelled out the effect of the strain hardening present in the base material. The effect was the decrease in hardness observed at room temperature, which, however, did not affect the strength parameters at elevated temperatures.

Acknowledgments

Work financed by the AGH University of Science and Technology statutory research number 16.16.180.006.

REFERENCES

1. Akca R., Gursel A. A review on superalloys and IN718 nickel-based INCONEL superalloy. Period. Eng. Nat. Sci. 2015; 3(1): 15–27. https://doi.org/10.21533/pen.v3i1.43
2. Hotlos A., Boczkal G., Nawrocki J., Ziewiec K. Microstructure of the oxide ceramics/Inconel 713C interface. Mater. Sci. Technol. 2019; 35(4): 456–461. https://doi.org/10.1080/02670836.2019.1570440
3. Darolia R. Development of strong, oxidation and corrosion resistant nickel-based superalloys: critical review of challenges, progress and prospects. Int. Mater. Rev. 2018; 64 (6): 1–26, https://doi.org/10.1080/09506608.2018.1516713
4. Perrut M., Caron P., Thomas M., Couret A. High temperature materials for aerospace applications: Ni-based superalloys and γ -TiAl alloys. C.R. Phys. 2018; 19(8): 657–671. https://doi.org/10.1016/j.crhy.2018.10.002
5. Morad A., Shash A. Nickel base superalloys used for aero engine turbine blades. Proceedings of the 16 th International Conference on Applied Mechanics and Mechanical Engineering (Int. AMME Conference), 27–29 May, 2014; 16(16): 1–22. https://doi.org/10.21608/amme.2014.35549
6. Gancarczyk K., Albrecht R., Kawalec M., Kościelniak B., Gradzik A., Szeliga D., Kawalec A., Ziaja W., Motyka M. The effect of re content on microstructure and creep resistance of single crystal castings made of nickel-based superalloys. Adv. Sci. Technol. Res. J. 2024; 18(1): 291–305. https://doi.org/10.12913/22998624/178463
7. Sonar T., Balasubramanian V., Malarvizhi S., Venkateswaran T., Sivakumar D. An overview on welding of Inconel 718 alloy - Effect of welding processes on microstructural evolution and mechanical properties of joints. Materials Characterization 2021; 174: 110997. https://doi.org/10.1016/j.matchar.2021.110997

8. Zhang H., Li C., Guo Q., Ma Z., Huang Y., Li H., Liu Y. Hot tensile behavior of cold-rolled Inconel 718 alloy at 650 °C: The role of δ phase. Mat. Sci. Eng. A 2018; 722: 136–146. https://doi.org/10.1016/j.msea.2018.02.093
9. Hosseini E., Popovich V.A. A review of mechanical properties of additively manufactured Inconel 718. Addit. Manuf. 2019; 30: 100877 https://doi.org/10.1016/j.addma.2019.100877
10. Meschut G., Hahn O., Janzen V., Olfermann T. Innovative joining technologies for multi-material structures. Weld. World 2014; 58: 65–75. https://doi.org/10.1007/s40194-013-0098-3
11. Hu A., Janczak-Rusch J., Sano T. Joining Technology Innovations at the Macro, Micro, and Nano Levels. Appl. Sci. 2019; 9(17), 3568–3576; https://doi.org/10.3390/app9173568
12. Braun M., Kellner L., Schreiber S., Ehlers S. Prediction of fatigue failure in small-scale butt-welded joints with explainable machine learning. Procedia Struct. Integr. 2022; 38: 182–191. https://doi.org/10.1016/j.prostr.2022.03.019
13. Boczkal, G., Dadun, K., Palka, P., Hotlos, A., Janoska, M., Structure and thermoelectric properties of Inconel 625/PT microjoint. Arch. Metall. Mater. 2019; 64(1): 197–200. https://doi.org/10.24425/amm.2019.126238
14. Saju T., Velu M. Review on welding and fracture of nickel based superalloys. Mater. Today Proc. 2021; 46(17): 7161–7169. https://doi.org/10.1016/j.matpr.2020.11.334
15. Winowlin Jappes J.T., Ajithram A., Adamkhan M., Reena D. Welding on Ni based super alloys – A review. Mater. Today Proc. 2022; 60 (3):1 656-1659. https://doi.org/10.1016/j.matpr.2021.12.208
16. Maurya A.K., Pandey C., Chhibber R. Dissimilar welding of duplex stainless steel with Ni alloys: A review. Int. J. Press. Vessels Pip. 2021; 192: 1044399. https://doi.org/10.1016/j.ijpvp.2021.104439
17. Mageshkumar K., Kuppan P., Arivazhagan N. Characterization of microstructure and mechanical properties of nickel based superalloy 617 by pulsed current gas tungsten arc welding technique. Mater. Res. Express 2018; 5: 066541. https://doi.org/10.1088/2053-1591/aacb56
18. Katarina R., Singh R. P., Sharma P., Phanden R.K. Welding of super alloys: A review Mater. Today Proc. 2021; 38(1): 265–268. https://doi.org/10.1016/j.matpr.2020.07.198
19. https://www.specialmetals.com/divisions/welding-products/tradenames/inconel/we112.pdf
20. Xie J., Ma Y., Xing W., Ou M., Zhang L., Liu K. Microstructure and mechanical properties of a new cast nickel-based superalloy K4750 joint produced by gas tungsten arc welding process. J. Mater. Sci. 2019; 54: 3558–3571. https://doi.org/10.1007/s10853-018-3081-y
21. Çoban O., Kaymak F., Gürol U., Koçak M. Characterization of fillet welded armor steel performed by robotic gas metal arc welding: effect of heat input on microstructure and microhardness. J. Mater. Eng. Perform. 2023; 34: 231–244. https://doi.org/10.1007/s11665-023-09058-y
22. Tharappel J.T., Babu J. Welding processes for Inconel 718 - A brief review. IOP Conf. Ser.: Mater. Sci. Eng. 2018; 330: 012082. https://doi.org/10.1088/1757-899X/330/1/012082
23. Sonar T., Balasubramanian V., Malarvizhi S., Venkateswaran T., Sivakumar D. An overview on welding of Inconel 718 alloy - Effect of welding processes on microstructural evolution and mechanical properties of joints. Materials Characterization 2021; 174: 110997. https://doi.org/10.1016/j.matchar.2021.110997
24. https://craigscottcapital.com/how-does-the-electrical-resistivity-of-inconel-718-change-with-temperature/
25. Marcos Ariel Mata-Rodríguez M.A., García-Rentería M.A., Ambríz-Rojas R.R., Cabral-Miramontes J.A., López-Morelos V.H., Ramírez-López M. Curiel-López F.F. Microstructural evolution of Inconel 718 during aging and its correlation with electric conductivity measurements. *Matls. Perf. Charact.* 2022; 11(1): 267–277. https://doi.org/10.1520/MPC20220035
26. https://www.upmet.com/sites/default/files/datasheets/718.pdf
27. Lee G.H., Kim B., Jeon J.B. Park M., Noh S., Kim B.J., Precipitate phase behavior and mechanical properties of Inconel 718 according to aging heat treatment time. Mater. Sci. Eng. A. 2025; 924: 147776. https://doi.org/10.1016/j.msea.2024.147776
28. Nunes R.M., Pereira D., Clarke T., Hirsch T. K. Delta Phase Characterization in Inconel 718 Alloys Through X-ray Diffraction. ISIJ Internat. 2015; 55(11): 2450–2454. http://dx.doi.org/10.2355/isijinternational.ISIJINT-2015-111
29. Chlebus E., Gruber K., Kuźnicka B., Kurzac J., Kurzynowski T. Effect of heat treatment on microstructure and mechanical properties of Inconel 718 processed by selective laser melting. *Mater. Sci. Eng. A 2015; 639:* 647–655. https://doi.org/10.1016/j.msea.2015.05.035